Morphology Controllable ZnO Growth on Facet-Controlled Epitaxial Lateral Overgrown GaN/Sapphire Templates

H. L. Zhou,[†] S. J. Chua,*[,‡] H. Pan,[†] Y. W. Zhu,[†] T. Osipowicz,[†] W. Liu,[‡] K. Y. Zang,[‡] Y. P. Feng,[†] and C. H. Sow[†]

Department of Physics, National University of Singapore, 2 Science Drive 3, 117542 Singapore, Republic of Singapore, and Institute of Materials Research and Engineering, 3 Research Link, 117602 Singapore, Republic of Singapore

Received: November 19, 2006; In Final Form: February 16, 2007

High-quality epitaxial ZnO layers grown on facet-controlled epitaxial lateral overgrown (FACELO) GaN/sapphire templates were achieved by an evaporation−physical transport−condensation method. The ZnO/FACELO GaN heterostructures showed a substantial improvement in the crystalline quality with a lower defect density and excellent photoluminescence emission. The effects of the growth temperature and oxygen flow rate on the morphology of ZnO were systematically studied. The determining factors for the formation of different morphologies were found to be gas-phase supersaturation and the surface energy of the growing planes. In addition, the lattice matching between the ZnO and GaN leads to the improvement of the electric and optical properties. With such kind of perfect ZnO/GaN heterostructure interfaces obtained on the semipolar $(11\bar{2}2)$ surface, the new opportunities for the fabrication of hybrid ZnO/GaN optoelectronic devices on sapphire are proposed.

1. Introduction

ZnO has attracted considerable attention over the past years owing to its attractive properties, such as good piezoelectric characteristics, chemical stability, and biocompatibility, and its potential applications in optoelectronic switches, high-efficiency photonic devices, near-UV lasers, and complex three-dimensional nanoscale systems.[1−4] In the previous works, sapphire has been used as the substrate to produce epitaxial ZnO films.[5−7] Recently, several groups reported the fabrication of n-ZnO/p-GaN electroluminescent devices and demonstrated the potential to realize photonic and electronic devices.[8,9] The quality of the ZnO films can be significantly improved because the lower lattices mismatch between the GaN and ZnO (∼1.9%). However, because of the high dislocation density (around 10^9-10^{10} cm^{-2}) in the GaN grown on c-sapphire, the as-grown ZnO films on *c*-GaN are well-known to contain higher defect densities, which are mainly threading dislocations. A technique that can help to overcome this problem is facet-controlled epitaxial lateral overgrowth (FACELO).[10−12] It is realized by starting the epitaxial growth on the (0001) plane and tuning the growth conditions to develop other facets, e.g., $(1\bar{1}01)$ and $(11\bar{2}2)$, on ELO stripes. Andeen et al. also reported the reduced dislocation of the ELO ZnO, which was grown on $MgAl_2O_4$ (111) substrate by the hydrothermal process.[13] Recently, Nishizuka et al.,[14] Ponce et al.,[15] and Neubert et al.[16] grew InGaN/GaN quantum well structures on the FACELO GaN templates, which led to higher internal quantum efficiency than those of the traditional *c*-plane due to the decrease of polarization. Narukawa et al. also proved that a higher quantum efficiency of the QWs was found on the $(11\bar{2}2)$ semipolar facets than on the (0001) polar surface.[17] However, the ZnO material has not attracted enough attention about this kind of combination. The ZnO films grown on the FACELO GaN templates will not only realize high crystal property but also achieve a reduced piezoelectric field on the ZnO/GaN heterointerface.

In this work, we successfully combined ZnO materials grown with the FACELO GaN templates. We reported the expitaxial overgrowth of ZnO films on facet-controlled ELO GaN/Sapphire (0001) templates by thermal evaporation with zinc vapor and oxygen as precursors. SiO_2 was chosen as the masking material to prevent nucleation of ZnO on it and the epitaxial phase was grown on the unmasked regions, forming a pattern of parallel strips on the substrate surface. With the increased growth temperature, the growth morphology of ZnO changes from long, needle-shaped nanorods to rectangular stripes with (0001) top facets and nonpolar $(11\bar{2}0)$ sidewalls, and finally to triangular stripes with $(11\bar{2}2)$ sidewalls. These results show that the ZnO growth facets can be controlled by the growth parameters and the overgrown region would achieve a reduced dislocation density in the entire epitaxial film. The X-ray diffraction (XRD), high-resolution transmission electron microscopy (HRTEM), room temperature photoluminescence (PL), and atom force microscopy (AFM) were used to characterize the ZnO films grown on the FACELO GaN templates. This method can be used to fabricate ZnO/GaN heterostructures with low dislocation densities, which may find important applications in future electronics and the fabrication of hybrid n-ZnO/p-GaN optoelectronic devices on sapphire.

2. Experimental Method

A 2 μm GaN film was first deposited by the EMCORE D180 MOCVD system on a *c*-plane sapphire substrate with low-temperature GaN as a buffer layer. Trimethyl-metals and ammonia (NH_3) were used as sources of Ga and N, respectively, with H_2 as carrier gas. A 100 nm SiO_2 mask was patterned into stripes oriented in the GaN $\langle 1\bar{1}00 \rangle$ direction, defining a 5 μm

* Address correspondence to this author. E-mail: elecsj@nus.edu.sg. Fax: +65-69820785.
[†] National University of Singapore.
[‡] Institute of Materials Research and Engineering.

10.1021/jp067682i CCC: $37.00
Published on Web 04/07/2007

wide opening with a period of 13 μm. GaN layers were grown via controlling the growth temperature and the reactor pressure by FACELO. The growth temperature and reactor pressure were 1000 °C and 200 Torr, respectively. The FACELO GaN/sapphire substrates were then put into a tube furnace to grow the ZnO films by thermal vaporization and condensation of Zn (99.99% purity) in the presence of oxygen. The alumina boat with Zn powder was placed at the center of a quartz tube and purged with helium (99.999% purity) at a flow rate of 100 sccm. The furnace temperature was increased to growth temperature, and an oxygen (99.99% purity) flow was introduced into the reactor. The mixed O_2 and He gas was maintained throughout the whole reaction process, which normally takes 30 min. The ZnO/GaN/sapphire layers were studied with SEM (JEOL JSM-6700F, 5kV), high-resolution XRD (Philips MRD system), high-resolution transmission electron microscopy (Philips CM300 FEG-TEM), micro-PL system (Renishaw, the PL spectra were recorded with use of a 325 nm excitation line with a lateral resolution of 2.0 μm), and AFM (Multimode-Digital Instruments).

3. Results and Discussion

3.1. Systematic Synthesis Study. Growth of ZnO is believed to be dominated by the vapor−solid (VS) process in the thermal evaporation method. Much work has been done both experimentally and theoretically on the kinetics of the whiskers growth.[18−20] The two-dimensional (2D) nucleation probability on the surface of a whisker was established to be

$$N_p = B \exp\left(-\frac{\pi\sigma^2}{k^2T^2 \ln S}\right) \quad (1)$$

where N_p is the nucleation probability, B is a constant, σ is the surface energy, k is the Boltzmann constant, T is the absolute temperature, and S is the gas-phase supersaturation ratio determined by $S = p/p_0$, where p is the actual vapor pressure and p_0 is the equilibrium vapor pressure corresponding to temperature T. The experiment parameters that could determine the morphology of the ZnO growth include the gas-phase supersaturation, the surface energy of the growth facets, the growth temperature, temperature gradient in the chamber, the heating rate, the gas flow rate, and the distance between the source materials and the substrate.

We kept all the other experiment parameters constant, and the dependence of the ZnO morphology on the growth temperature and oxygen flow rate was systematically studied. Figure 1 displays the morphological structures of ZnO dependence on the growth temperature and oxygen flow rate. First, according to the different growth temperatures of the ZnO growth, it can be divided into three regions. In region I (T < 800 °C), the as-grown ZnO forms long needle-shaped nanorods with a typical diameter of around 100 nm and 7 μm height on the GaN template due to the very high growth rate in the c-direction and the poor surface migration of Zn atoms on the (0001) surface at low temperatures. In region II, with the increasing growth temperature, the side walls change from vertical nonpolar $(11\bar{2}0)$ facets to inclined $(11\bar{2}2)$ facets. The uniform and rectangular shape ZnO structures were observed in this region. However, only a small growth temperature vs flow rate region can achieve the smooth (0001) surface. The morphology changes with growth temperature from 800 to 810 °C, and there are some intermediate growth regimes whereby both the $(11\bar{2}0)$ and the $(11\bar{2}2)$ facets are formed. It was noted that the $(11\bar{2}2)$ surface area keeps increasing while the $(11\bar{2}0)$ surface is disappearing with the higher growth temperature. In region III, at higher temperatures, the inclined $(11\bar{2}2)$ surface becomes rough due to the increase in the evaporation rate of absorbed source molecules on that surface. The variations of the 2D nucleation probability on the different facets were studied to investigate the mechanism behind these observations. According to eq 1, higher temperature increases the gas-phase pressure of ZnO,[20] which means higher supersaturation. Therefore, higher temperature introduces a higher 2D nucleation probability. On the other hand, the surface energy is related to the crystal plane: a low miller index crystal surface is of lower surface energy.[20] The lower surface energy leads the larger 2D probability of nucleation. Meanwhile, an atom absorbed on a low-energy surface has low binding energy and a high probability of desorption.[21] Competition between the supersaturation and surface energy is responsible for the temperature dependence of the ZnO morphology. At lower temperature, a lower millier index plane achieves larger 2D probability of nucleation due to the lower probability of desorption. As a result, the growth rate on the [0001] direction is relatively higher and keeps suppressing the other facet's growth rate like $\{11\bar{2}2\}$ and $\{11\bar{2}0\}$, thus the ZnO nanorods structures with lower volume ZnO were grown on the GaN. When the growth temperature increases, the volume of ZnO grown on the GaN is larger corresponding to the increased supersaturation. However, the higher temperature will also induce larger desorption probability of the adatoms on the (0001) surface, which results in lower growth rate on the c-plane. Meanwhile, the temperature dependence of the growth rate on the $\{11\bar{2}2\}$ and $\{11\bar{2}0\}$ facets is hard to investigate. The competitive capturing of the adatoms is more dominant among these three different facets, when the crystal has several fast growth directions. For example, the $\{0001\}$ and $\{11\bar{2}2\}$ are the fast growth surfaces of the ZnO crystal.[22] According to the research work on the growth rates about the FACELO GaN of different facets,[11] and due to the structural similarity between GaN and ZnO, we could reasonably assume that the ZnO $\{11\bar{2}0\}$ growth rate will increase when the temperature is higher. In particular, at region II the increasing temperature causes a higher growth rate on the $\{11\bar{2}0\}$ facets, but the growth rate on the $\{11\bar{2}0\}$ surface is still competing with that of the $\{11\bar{2}2\}$ facets. When the temperature increased to 800 °C, the $\{11\bar{2}0\}$ facets appear. As the temperature becomes higher (>800 °C), the $\{11\bar{2}0\}$ growth rate keeps increasing. Eventually the $\{11\bar{2}2\}$ facets appear instead of the $\{11\bar{2}0\}$ facets as the growth rate on the $\{11\bar{2}0\}$ facets suppresses that of the $\{11\bar{2}2\}$ plane. This also should be due to the difference of the stability of each surface, which mainly depends on the surface energy. It could be deduced that the ZnO $(11\bar{2}2)$ facets are energetically more stable than the $\{11\bar{2}0\}$ facets. When we account for the ZnO growth volume as the variation of temperature, the changes in the growth rate of all three different facets should be included. The final morphology of the ZnO is the result of the competition amongthe growth rate of these facets.

Second, when we keep the growth temperature constant and change the oxygen flow rate, different growth rates on the $(11\bar{2}2)$ and (0001) facets were observed with various oxygen flow rates, as shown in Figure 1. At the low oxygen flow rate (5 sccm), the result is low supersaturation, thus the volume of the growth of ZnO is quite small. As we keep increasing the oxygen flow rate, the supersaturation will be increased.[20] Therefore, the increasing oxygen flow rate introduces the higher supersaturation corresponding to the larger volume of the growth ZnO, as shown in Figure 1. For the constant temperature, the desorption probability of adsorb atoms will not change. So the (0001)

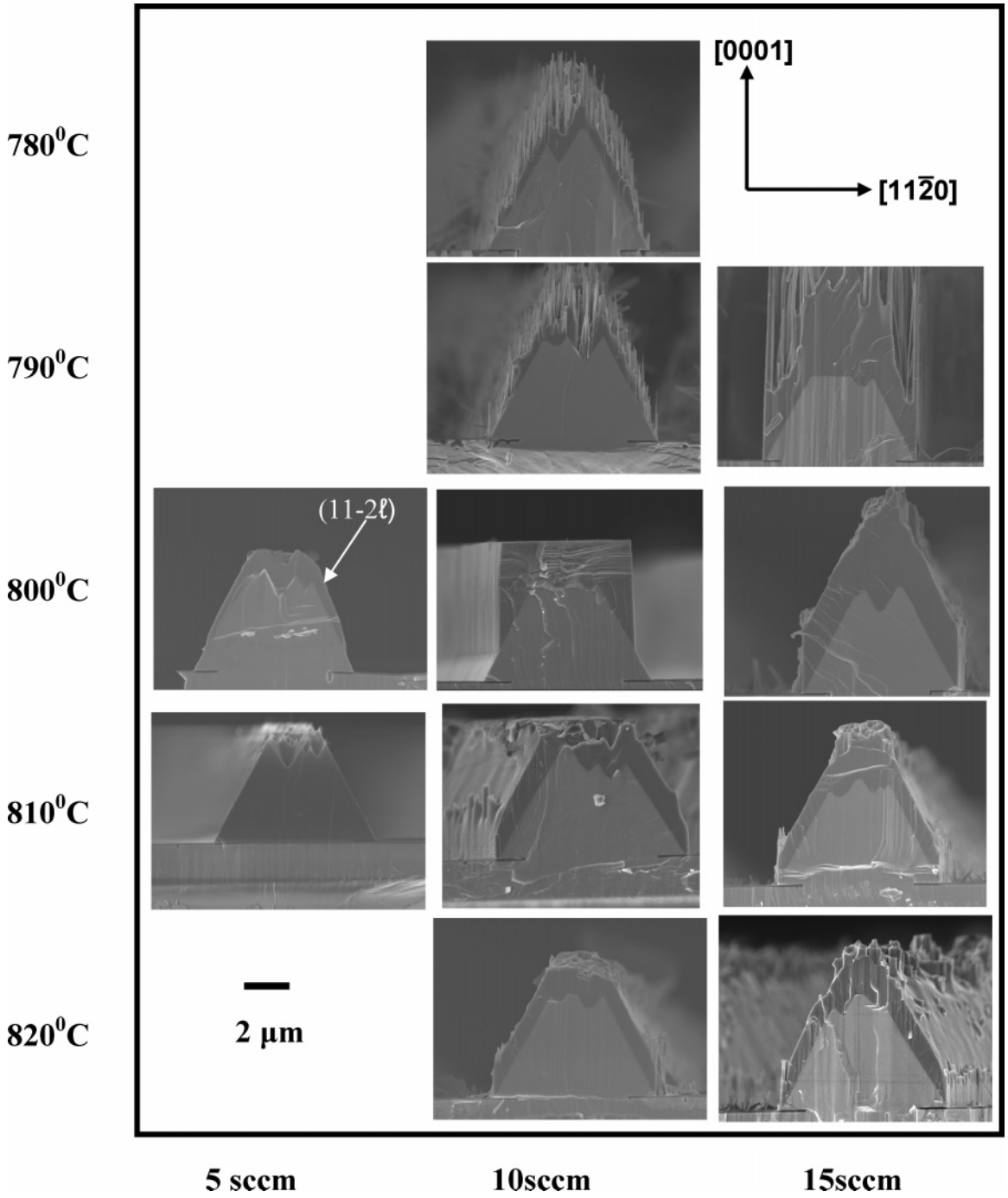

Figure 1. Morphological changes in ZnO grown on the FACELO GaN templates with different growth temperature and oxygen flow rate. Growth time was 0.5 h.

surface with lower surface energy will lead to the higher growth rate with higher oxygen flow rate, which is further verified by the morphology changes observed in Figure 1. Therefore, the increasing oxygen flow rate has an opposite effect on the [0001] growth rate compared to the higher growth temperature. On the basis of the preview discussions, the surface energy and the supersaturation are two dominant growth factors in controlling the morphology of the ZnO in the VS growth process.

3.2. Electron Microscope Characterization on the ZnO Grown on FACELO GaN Templates. The microstructure of the top layer and the nature of the epitaxial growth of ZnO films grown at 800 °C with an oxygen flow rate of 10 sccm were further investigated by HRTEM. Figure 2a shows a HRTEM image of the ZnO/FACELO GaN interface. The lattice fringes of ZnO are perfectly aligned with those of the GaN and the interface is sharp on the atomic level. The selected area electron diffraction (SAED) pattern taken near the GaN/ZnO interface (inset in Figure 2a) indicates near lattice matching between ZnO and GaN hexagonal structures, which allow the perfect epitaxial growth of ZnO on GaN and thus a high crystal quality. A cross-sectional TEM image with lower magnification is presented in Figure 2b to further show the interface of the ZnO/FACELO GaN on a large area. The ELO GaN dislocations have been studied by several groups[23−25] and the formation of the horizontal dislocations (HDs) can dramatically decrease the threading dislocation (TD) density of the regrown GaN regions. In Figure 2b, we can see that the laterally overgrown ZnO is essentially including the HDs. The effect of dislocation bending can be understood by considering the energy of dislocation lines emerging from the free surface of a crystal.[26] From the point

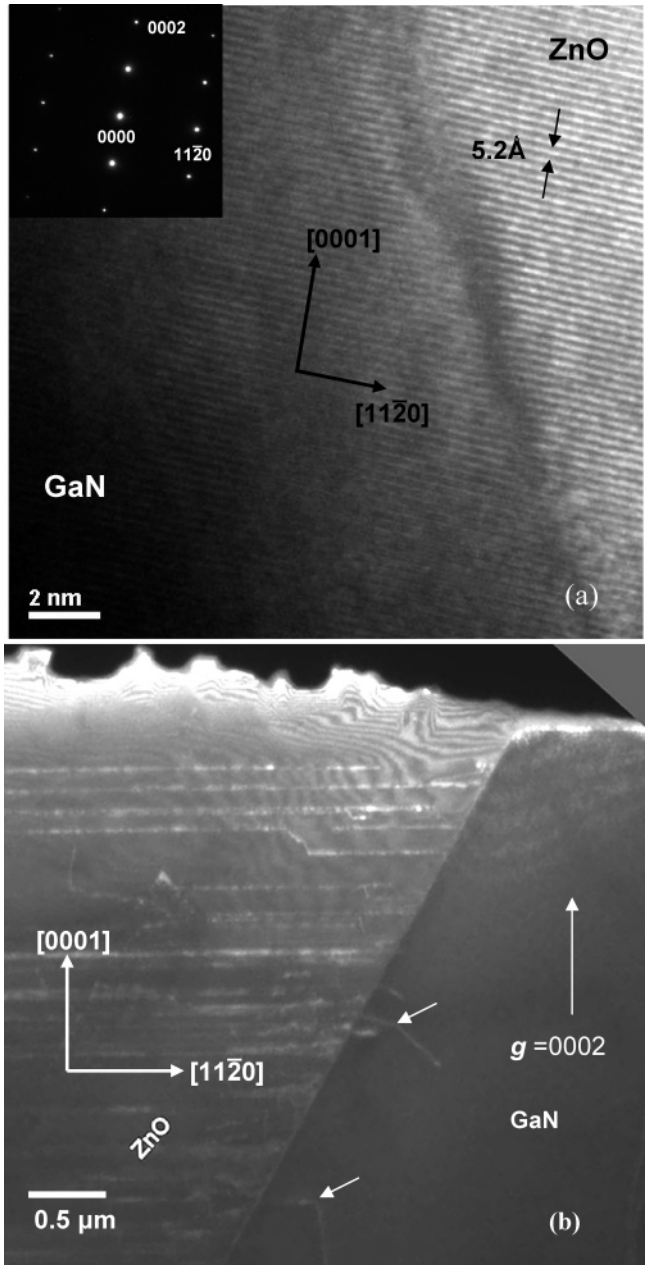

Figure 2. (a) HRTEM image and the corresponding SAED pattern of ZnO/FACELO GaN interface grown at 800 °C with the oxygen flow rate 10 sccm. (b) Cross-sectional TEM image with $g = 0002$ near the interface of ZnO/FACELO GaN grown at 800 °C with the oxygen flow rate 10 sccm.

of view of the dislocation line tension, any dislocation would tend to become perpendicular to a free surface to diminish its energy. As a result, dislocations would gradually change their line directions toward the normal direction of the current facet plane, as can be seen in Figure 2b (indicated by arrows). All the observed dislocations in ZnO are parallel toward the mask areas and no vertical dislocation propagations to the ZnO surface were obtained in the overgrowth region. High-quality wing regions have been realized by the growth of ZnO (11$\bar{2}$0) vertical sidewalls. This strongly suggests that high-quality ZnO films can be pseudomorphically grown on the FACELO GaN, as shown in Figure 1.

3.3. XRD Characterization on the ZnO Grown on FACELO GaN Templates. Figure 3 shows the HRXRD $2\theta/\omega$ scans of the ZnO samples grown at different growth temperatures with the same oxygen flow rate of 10 sccm. Here, we have shown

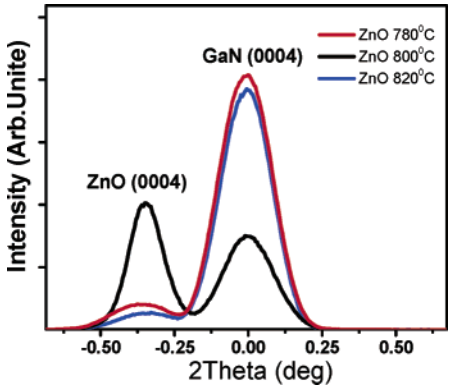

Figure 3. The X-ray diffraction $\omega/2\theta$ scan of the epi-ZnO/FACELO GaN/sapphire (0001) heterostructure grown at different temperatures with the same oxygen flow rate of 10 sccm.

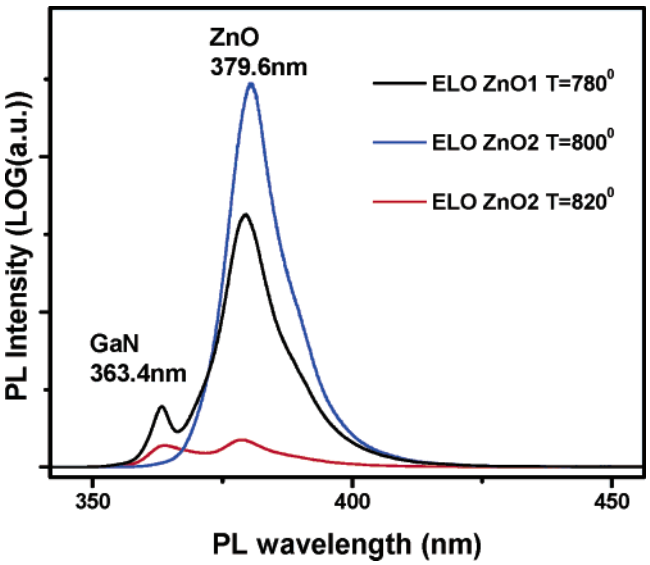

Figure 4. The micro-PL spectra were taken from three different ZnO/FACELO GaN samples grown at different temperatures with the same oxygen flow rate of 10 sccm and excitation by 325 nm laser.

the ZnO (0004) and GaN (0004) diffraction peaks that indicate the *c*-axis-oriented ZnO growth with wurtzite structure. XRD rocking curves were measured to determine the degree of alignment to the normal direction of the substrate surface. The narrowest full width at half-maximum (fwhm) of 0.12° was observed on ZnO grown at 800 °C compared to the 0.14° for the nanorods ZnO grown at 780 °C and 0.19° for the ZnO grown at 810 °C. This shows that the ZnO layers grown at 800 °C are well oriented along the (0001) direction with improved crystalline properties. However, the larger fwhm obtained on the ZnO nanorods grown at 780 °C may not indicate the lower crystal quality of the ZnO nanostructures and it could be introduced by the orientation and uniformity of the nanorods. Furthermore, the highest intensity of the ZnO (0004) diffraction peak of ZnO films grown at 800 °C indicates the best crystalline quality compared to the thin films grown at higher temperatures with a high density of point and line defects. A reduction in the thickness of the films grown at higher temperatures also led to a decrease in the XRD peak intensity. From Figure 3, we can also observe that the ZnO (0004) spectrum from the nanorods structure shows a substantial peak shift when compared to the thin films. This is caused by the strain relaxation in high-aspect-ratio structures.[27] However, the ZnO thin film samples show an in-plane tensile stress component as confirmed from XRD analysis.

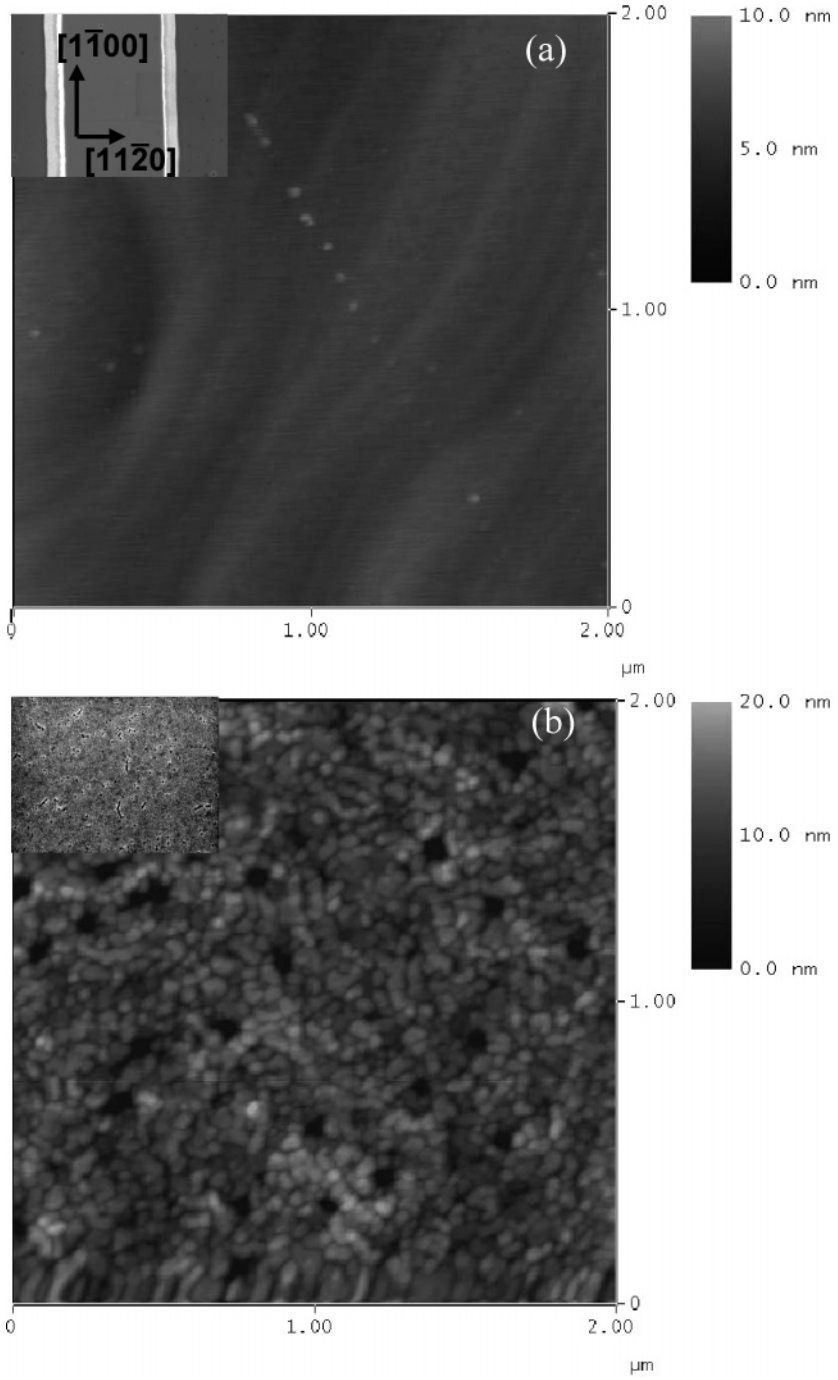

Figure 5. (a) The surface morphology of the 800 °C ZnO/FACELO GaN sample, which was characterized by AFM with (b) a control sample grown on c-GaN at the same growth conditions for comparison.

3.4. Optical Property of the ZnO Grown on FACELO GaN Templates. The optical properties of the ZnO layers on FACELO GaN were investigated by room temperature micro-PL spectroscopy. All these ZnO samples were grown with the same oxygen flow rate of 10 sccm. In our PL system, the wavelength of He−Cd laser used is 325 nm. The absorption coefficient α of ZnO films can be determined from transmittance measurements,[28] which is around 3.3×10^{-3} nm^{-1} at room temperature. This means that within the 300 nm ZnO layer the intensity of the PL excitation laser will be reduced by e^{-1}, so most of incident energy should be absorbed by ZnO. Obviously from Figure 1, the ratio of the GaN peak intensity to that of ZnO is seen to vary with the growth temperature, indicating different thickness or/and crystal properties of ZnO layers. In the PL spectra (Figure 4), the peaks from GaN and ZnO can be seen at around 363 and 380 nm, respectively. From the spectra of the 780 °C ZnO/FACELO GaN sample, the GaN/ZnO intensity ratio larger than one may suggest that the thickness of the ZnO layer is no larger than 300 nm or the as-grown ZnO is the nanorod, as observed from the SEM images (Figure 1). The strongest PL intensity of the ZnO is observed from the 800 °C grown ZnO/FACELO GaN with the full width at half-maximum (fwhm) of the PL ZnO peak of about 10 nm, which is the narrowest fwhm of three ZnO samples from different temperatures. This implies a higher epitaxial crystalline quality of ZnO films grown at 800 °C. The spectrum of 820 °C ELO ZnO/GaN showed the degraded crystalline with the broadening of the ZnO peak (around 23 nm). The PL spectra indicate that the best ZnO quality is achieved at 800 °C grown with the oxygen flow rate of 10 sccm.

3.5. Surface Roughness Characterization of ZnO Grown on FACELO GaN Templates. The surface morphology of the overgrowth ZnO sample grown at 800 °C with the oxygen flow rate of 10 sccm was characterized by AFM compared to a control sample grown on *c*-GaN under the same growth conditions, as shown in Figure 5. The surface roughness (rms) of the epi-ZnO on FACELO GaN and control sample is 0.40 and 3.67 nm, respectively. Atomic steps and terraces were clearly observed from the surface of the ZnO grown on the FACELO GaN templates. Only a few step terminations in AFM observations can be detected, which indicates a high quality of the overgrown sample once more. The surface pit density of the overgrown GaN sample is reduced by more than 100 times, compared with the control sample. This should be induced by two reasons. First, the lower dislocation density and higher crystal property was achieved by the FACELO method. Second, maybe the growth parameter of ZnO layers used is preferred for the FACELO GaN templates rather than *c*-plane GaN. All these observations support that the ZnO growth method on $(11\bar{2}2)$ facets has an obvious beneficial effect on the dislocation behavior in the ZnO layer grown on *c*-plane GaN templates.

4. Conclusion

In summary, high-quality epitaxial ZnO/FACELO GaN heterostructures have been grown on sapphire substrates. These heterostructures showed a substantial improvement in the crystalline quality with a lower defect density and excellent photoluminescence emission. Different facet growth rates can be controlled by the processing parameters, such as the temperature and oxygen flow rate. In addition, the achievement of the perfect ZnO/GaN interfaces grown on the semipolar surface will provide novel opportunities for the fabrication of hybrid ZnO/GaN optoelectronic devices on sapphire.

Acknowledgment. The authors acknowledge support from the NUS Academic Research Fund. We would like to thank Ms. Chow Shue Yin, Ms. Yong Anna Marie, and Dr. Tripathy Sudhiranjan for their help on characterizations.

References and Notes

(1) Xia, Y. N.; Yang, P. D.; Sun, Y.; Wu, Y.; Mayers, B.; Yin, Y.; Kim, F.; Yan, H. *Adv. Mater.* **2003**, *15*, 353.

(2) Pan, Z. W.; Dai, Z. R.; Wang, Z. L. *Science* **2001**, *291*, 1947.

(3) Gao, P.; Wang, Z. L. *J. Phys. Chem. B* **2002**, *106*, 12658.

(4) Chen, C. S.; Kuo, C. T.; Wu, T. B.; Lin, I. N. *Jpn. J. Appl. Phys.* **1997**, *36*, 1169.

(5) Kawasaki, M.; Ohtomo, A.; Koinuma, H.; Sakurai, Y.; Yoshida, Y.; Tang, Z. K.; Yu, P.; Wang, G. K. L.; Segawa, Y. *Mater. Sci. Forum* **1998**, *264*, 1459.

(6) Bagnall, D. M.; Chen, Y. F.; Zhu, Z.; Yao, T.; Koyama, S.; Shen, M. Y.; Goto, T. *Appl. Phys. Lett.* **1997**, *70*, 2230.

(7) Srikant, V.; Sergo, V.; Clarke, D. R. *J. Am. Ceram. Soc.* **1995**, *78*, 1931.

(8) Vispute, R. D.; Talyansky, V.; Choopun, S.; Sharma, R. P.; Venkatesan, T.; He, M.; Tang, X.; Halpern, J. B.; Spencer, M. G.; Li, Y. X.; Salamanca-Riba, L. G.; Iliadis, A. A.; Jones, K. A. *Appl. Phys. Lett.* **1998**, *73*, 348. Alivov, Y. I.; Van Nostrand, J. E.; Look, D. C.; Chukichev, M. V.; Ataev, D. M. *Appl. Phys. Lett.* **2003**, *83*, 2943.

(9) Rogers, D. J.; Teherani, F. H.; Yasan, A.; Minder, K.; Kung, P.; Razeghi, M. *Appl. Phys. Lett.* **2006**, *88*, 347.

(10) Miyake, H.; Motogaito, A.; Hiramatsu, K. *Jpn. J. Appl. Phys.* **1999**, *38*, L1000.

(11) (a) Hiramatsu, K.; Nishiyama, K.; Onishi, M.; Mizutani, H.; Narukawa, M.; Motogaito, A.; Miyake, H.; Iyechika, Y.; Maeda, T. *J. Cryst. Growth* **2000**, *221*, 316. (b) Miyake, H.; Narukawa, M.; Hiramatsu, K.; Naoi, H.; Iyechika, Y.; Maeda, T. *Phys. Status Solidi A* **2001**, *188*, 725.

(12) Vennégués, P.; Beaumont, B.; Bousquet, V.; Vaille, M.; Gibart, P. *J. Appl. Phys.* **2000**, *87*, 4175

(13) Andeen, D.; Kim, J. H.; Lange, F. F.; Goh, G. K. L.; Tripathy, S. *Adv. Funct. Mater.* **2006**, *16*, 799.

(14) Nishizuka, K.; Funato, M.; Kawakami, Y.; Fujita, S.; Narukawa, Y.; Mukai, T. *Appl. Phys. Lett.* **2004**, 85, 3122.

(15) Srinivasan, S.; Stevens, M.; Ponce, F. A.; Mukai, T. *Appl. Phys. Lett.* **2005**, *87*, 131911.

(16) Neubert, B.; Brückner, P.; Habel, F.; Scholz, F.; Riemann, T.; Christen, J.; Beer, M.; Zweck, J. *Appl. Phys. Lett.* **2005**, *87*, 182111.

(17) Funato, M.; Kotani, T.; Kondou, T.; Kawakami, Y.; Narukawa, Y.; Mukai, T. *Appl. Phys. Lett.* **2006**, *88*, 261920.

(18) (a) Burton, W. K.; Cabrera, N.; Frank, F. C. *Nature* **1949**, 163, 398−399. (b) Burton, W. K.; Cabrera, N.; Frank, F. C. *Philos. Trans. R. Soc. London, Ser. A* **1951**, *243*, 299−358.

(19) (a) Sears, G. W. *Acta Metall.* **1955**, 3, 361−366. (b) Sears, G. W. *Acta Metall.* **1955**, *3*, 367−369.

(20) (a) Zu, R. D.; Zheng, W.; Wang, Z. L. *Adv. Funct. Mater.* **2003**, 13, 9−24. (b) Coleman, R. V.; Sears, G. W. *Acta Metall.* **1957**, *5*, 131−136. (c) Parker, R. L. *J. Chem. Phys.* **1962**, *37*, 1600−1605. (d) Ye, C.; Fang, X.; Hao, Y.; Teng, X.; Zhang, L. *J. Phys. Chem. B* **2005**, *109*, 19758−19765.

(21) Lews, B. In *Crystal Growth*;Pamplin, B. R., Ed.; Pergamon: Oxford, UK, 1980, pp 23−63.

(22) Ng, H. T.; Li, J.; Smith, M. K.; Nguyen, P.; Gassell, A.; Han, J.; Meyyappan, M. *Science* **2003**, *300*, 1249−1249.

(23) Zheleva, T. S.; Nam, O. H.; Bremser, M. D.; Davis, R. F. *Appl. Phys. Lett.* **1997**, *71*, 2472.

(24) Kuwano, N.; Horibuchi, K.; Kagawa, K.; Nishimoto, S.; Sueyoshi, M. *J. Cryst. Growth* **2002**, *237−239*, 1047.

(25) Ishida, M.; Ogawa, M.; Orita, K.; Imafuji, O.; Yuri, M.; Sugino, T.; Itoh, K. *J. Cryst. Growth* **2000**, *221*, 345.

(26) Hirth, J. P.; Lothe, J. *Theory of Dislocations*, 2nd ed.; Wiley: New York, 1982.

(27) Cong, G. W.; Wei, H. Y.; Zhang, P. F.; Peng, W. Q.; Wu, J. J.; Liu, X. L.; Jiao, C. M.; Hu, W. G.; Zhu, Q. S.; Wang, Z. G. *Appl. Phys. Lett.* **2005**, *87*, 231903.

(28) GÜMÜ, C.; Ozkendir, O. M.; Kavak, H.; Ufuktepe, Y. *J. Optoelectron. Adv. Mater.* **2006**, *8*, 299.